Using Landsat-derived disturbance and recovery history and lidar to map forest biomass dynamics

Citation	Pflugmacher, D., Cohen, W. B., Kennedy, R. E., & Yang, Z. (2014). Using Landsat-derived disturbance and recovery history and lidar to map forest biomass dynamics. Remote Sensing of Environment, 151, 124-137. doi:10.1016/j.rse.2013.05.033
DOI	10.1016/j.rse.2013.05.033
Publisher	Elsevier
Version	Version of Record
Terms of Use	http://cdss.library.oregonstate.edu/sa-termsofuse

Remote Sensing of Environment 151 (2014) 124–137

Contents lists available at ScienceDirect

Remote Sensing of Environment

journal homepage: www.elsevier.com/locate/rse

Using Landsat-derived disturbance and recovery history and lidar to map forest biomass dynamics

Dirk Pflugmacher [a,*], Warren B. Cohen [b], Robert E. Kennedy [c], Zhiqiang Yang [a]

[a] Department of Forest Ecosystems and Society, Oregon State University, 321 Richardson Hall, Corvallis, OR 97331, USA
[b] USDA Forest Service, Pacific Northwest Research Station, Forestry Sciences Laboratory, 3200 SW Jefferson Way, Corvallis, OR 97331, USA
[c] Department of Earth and Environment, Boston University, 675 Commonwealth Ave, Boston, MA 02215, USA

ARTICLE INFO

Article history:
Received 5 September 2012
Received in revised form 18 May 2013
Accepted 21 May 2013
Available online 8 October 2013

Keywords:
Landsat
Time series
Forest disturbance
Biomass
Carbon
Lidar
Tasseled cap
LandTrendr

ABSTRACT

Improved monitoring of forest biomass and biomass change is needed to quantify natural and anthropogenic effects on the terrestrial carbon cycle. Landsat's temporal and spatial coverage, moderate spatial resolution, and long history of earth observations provide a unique opportunity for characterizing vegetation changes across large areas and long time scales. However, like with other multi-spectral passive optical sensors, Landsat's relationship of single-date reflectance with forest biomass diminishes under high leaf area and complex canopy conditions. Because the condition of a forest stand at any point in time is largely determined by its disturbance and recovery history, we conceived a method that enhances Landsat's spectral relationships with biomass by including information on vegetation trends prior to the date for which estimates are desired. With recently developed algorithms that characterize trends in disturbance (e.g. year of onset, duration, and magnitude) and post-disturbance regrowth, it should now be possible to realize improved Landsat-based mapping of current biomass across large regions. Moreover, given that we now have 40 years of Landsat data, it should also be possible to use this approach to map historic biomass densities.

In this study, we developed regression tree models to predict current forest aboveground biomass (AGB) for a mixed-conifer region in eastern Oregon (USA) using Landsat-based disturbance and recovery (DR) metrics. We employed the trajectory-fitting algorithm LandTrendr to characterize DR trends from yearly Landsat time series between 1972 and 2010. The most important DR predictors of AGB were associated with magnitude of disturbance, post-disturbance condition and post-disturbance recovery, whereas time since disturbance and pre-disturbance trends showed only weak correlations with AGB. Including DR metrics substantially improved predictions of AGB (RMSE = 30.3 Mg ha^{-1}, 27%) compared to models based on only single-date reflectance (RMSE = 39.6 Mg ha^{-1}, 35%). To determine the number of years required to adequately capture the effect of DR on AGB, we explored the relationship between time-series length and model prediction accuracy. Prediction accuracy increased exponentially with increasing number of years across the entire observation period, suggesting that in this forest region the longer the historic record of disturbance and recovery metrics the more accurate the mapping of AGB. However, time series lengths of between 10 and 20 years were adequate to significantly improve model predictions, and lengths of as little as 5 years still had a meaningful impact. To test the concept of historic biomass prediction, we applied our model to Landsat time series from 1972–1993 and estimated AGB biomass change between 1993 and 2007. Our estimates compared well with historic inventory data, demonstrating that long-term Landsat observations of DR processes can aid in monitoring AGB and AGB change.

Instead of directly linking Landsat data with the limited amount of available field-based AGB data, in this study we used the field data to map AGB with airborne lidar and then sampled the lidar data for model training and error assessment. By using lidar data to build and test our prediction model, this study illustrates that lidar data have great value for scaling between field measurements and Landsat data.

1. Introduction

Improved monitoring of forest biomass is required to understand the role of forest ecosystems in the global climate and to implement national and international mitigation strategies that reduce greenhouse gas emissions (Aber et al., 2001; Bonan, 2008; Houghton, 2005). Current observations of the land–atmosphere C-flux based on measurements via eddy covariance techniques (Baldocchi, 2003) and field inventories (Goodale et al., 2002) are too sparse in time and space to allow inferences of terrestrial carbon sources and sinks with sufficient accuracy (Denman et al., 2007; Houghton, Hall, & Goetz, 2009). Consequently, the value of remote sensing data for estimating forest aboveground biomass (AGB) is high.

* Corresponding author at: Department of Geography, Humboldt-Universität zu Berlin, Unter den Linden 6, 10099 Berlin, Germany.
E-mail address: dirk.pflugmacher@geo.hu-berlin.de (D. Pflugmacher).

0034-4257/$ – see front matter © 2013 Elsevier Inc. All rights reserved.
http://dx.doi.org/10.1016/j.rse.2013.05.033

The most promising strategies for improving forest carbon estimates with remote sensing data are to combine them with ecosystem process models. For example, studies have combined ecosystem process models with maps of disturbance history and age from Landsat time series (Cohen, Harmon, Wallin, & Fiorella, 1996; Masek & Collatz, 2006), and with satellite-based estimates of FPAR (fraction of photosynthetic active radiation) (Coops & Waring, 2001; Smith, Knorr, Widlowski, Pinty, & Gobron, 2008). Ecosystem models are valuable because they can provide a detailed simulation of ecophysiological processes, including those below ground, and can be run in prognostic mode, e.g. to analyze ecosystem feedbacks to future climate scenarios. However, these models also require large, detailed datasets for parameterization, and independent validation is limited. In addition, over decadal time scales, carbon fluxes are largely driven by changes in tree biomass, successional change in forest composition, and disturbance events; processes that are not well represented by current ecosystem models (Urbanski et al., 2007). Remote sensing has the potential to provide much of the detailed information that such models require.

Lidar (light detection and ranging) is currently the only sensor type whose signal does not saturate in high biomass forests (e.g. 1200 Mg ha^{-1}, Lefsky, Cohen, Parker, & Harding, 2002); thus lidar data are ideal for mapping AGB. Lidar measures the three-dimensional distribution of tree heights and foliage (Drake et al., 2002; Lefsky et al., 1999) resulting in accurate estimates of forest biomass across a broad range of forest types and biomes (Dubayah et al., 2010; Lefsky et al., 2002). Lidar systems are currently available either as wall-to-wall scanners (most operational airborne systems) or as discrete samplers with ground footprints between 10 and ~65 m in diameter (Abshire et al., 2005; Blair, Rabine, & Hofton, 1999; Nelson, Krabill, & Tonelli, 1988). Several studies have now demonstrated how to integrate large footprint lidar samplers and satellite imagery to map forest biomass over temperate (Lefsky, Turner, Guzy, & Cohen, 2005), boreal (Boudreau et al., 2008), and tropical forests (Baccini et al., 2012; Helmer, Lefsky, & Roberts, 2009; Saatchi et al., 2011). Estimating biomass with airborne laser scanning data is often more accurate (Zolkos, Goetz, & Dubayah, 2013), but the high acquisition costs and data volumes currently prohibit repeated monitoring of large areas. Thus, recent research with airborne data has increasingly focused on integrating lidar with forest inventory data in multi-stage sampling frameworks (Andersen, 2009; Gregoire et al., 2011; Stephens et al., 2012), and also with satellite imagery (Andersen, Strunk, Temesgen, Atwood, & Winterberger, 2011; Wulder & Seemann, 2003). To effectively use lidar as a sampling tool in regional vegetation studies it is of interest to examine how the choice of sampling design and sampling density can reduce uncertainties in the estimates.

Multi-spectral satellite sensors provide frequent and consistent observations of the earth's surface, and have been used extensively for monitoring vegetation characteristics across a variety of spatial and temporal scales (Cohen & Goward, 2004; Running et al., 2004). As a result, a large body of research has focused on estimating biomass directly with moderate spatial resolution (e.g. Landsat, Hall, Skakun, Arsenault, & Case, 2006; Powell et al., 2010) and coarse resolution sensor data (e.g. MODIS, Baccini, Friedl, Woodcock, & Warbington, 2004; Blackard et al., 2008). To estimate AGB, these studies often utilize empirical models based on single-date reflectance and field measurements. However, the signal recorded by passive optical multi-spectral sensors is known to saturate under closed canopy conditions (Lu, 2006) diminishing the accuracy of biomass estimates obtained from these sensors in medium to high biomass forests (e.g. > ~150 Mg ha^{-1}).

Despite this limitation, estimating AGB with multi-spectral sensors remains an active field of research. Approaches that rely solely on regional statistics and thematic land cover data may greatly misrepresent the actual spatial distribution of AGB (Goetz et al., 2009). Recently, Avitabile, Herold, Henry, and Schmullius (2011) compared available biomass maps for Uganda and found, while estimates obtained from multi-spectral data and regression models were conservative, maps based on biome-average values and national land cover data vastly overestimated AGB. To improve AGB estimates with multi-spectral data, scientists have tested a variety of modeling techniques (Hudak, Lefsky, Cohen, & Berterretche, 2002; Powell et al., 2010), utilized multiple intra-annual imagery (Lefsky, Cohen, & Spies, 2001) and inter-annual time series (Helmer et al., 2010), and included topographic and climate variables in addition to spectral variables (Baccini et al., 2004; Powell et al., 2010) with mixed success.

One potential means of enhancing the relationship between Landsat reflectance and AGB is by incorporating Landsat spectral trends of disturbance and recovery (DR) prior to the date for which predictions are desired (Pflugmacher, Cohen, & Kennedy, 2012). The conceptual basis for combining DR metrics with spectral data derives from ecological observations that type (e.g. fire, harvest, insect) and intensity of disturbances influence forest structure, composition, and carbon dynamics (Franklin et al., 2002; Halpern, 1988; Harmon, Ferrell, & Franklin, 1990; Spies, 1998). Disturbance type and severity influence the proportion of live biomass that combusts during a fire, is transferred to dead woody biomass or removed from a site as products (Kasischke et al., 2005). In combination with environmental factors, disturbances determine the rate and pathways of subsequent recovery (Gough, Vogel, Harrold, George, & Curtis, 2007; Meigs, Donato, Campbell, Martin, & Law, 2009), resulting in highly variable spatial and temporal patterns of forest regrowth (Halpern, 1988; Yang, Cohen, & Harmon, 2005).

Recently, we tested the DR approach for predicting AGB with good success (Pflugmacher et al., 2012). Including DR metrics calculated from yearly Landsat time series (1972–2010) into empirical models improved prediction accuracy substantially; root mean square error (RMSE) decreased from 57% to 41% compared to models that used only single-date (SD) Landsat data. However, the study was a proof-of-concept and limited to 51 field plots and manually-digitized trajectories. Here, our objective was to extend that work to map AGB and AGB change (ΔAGB). Accomplishing this required that we: 1) automate the characterization of DR metrics, 2) develop DR-based AGB models, 3) and test if those models can be used to predict historic AGB and ΔAGB. Further, we wanted to explore the use of airborne lidar for training statistical models that are better representative of the wide range of forests and disturbance regimes in the study area than were a limited sample of field measurements. Thus, instead of using the field plots from our previous study directly for model training, we use these plots to create a high-resolution AGB surface predicted from airborne lidar data. We then sample the lidar-based AGB predictions and quantify the effect of sampling density on the prediction accuracy of the DR models.

2. Methods

2.1. Study area

The study area is located in the Blue Mountains of eastern Oregon, USA (Fig. 1). The area is ~830 km^2 and covers two large watersheds of the Upper Middle Fork John Day River. Current forest structure has been shaped by natural and anthropogenic disturbances, with harvest, insects, and fire as major agents. Mountain pine beetle (*Dendroctonus ponderosae* Hopkins) and western spruce budworm (*Choristoneura occidentalis* Freeman) are the main causes of tree mortality and defoliation (Meigs, Kennedy, & Cohen, 2011). Thinning harvest and frequent low intensity fire are common, which have created structurally and compositionally complex mixed and multi-aged conifer-dominated forests (Campbell & Liegel, 1996). Two high intensity wildfires have been documented by the Monitoring Trends in Burn Severity (MTBS) project (http://www.mtbs.gov/). The larger fire burned approximately 14,800 ha in 1996 in the northern part, and the smaller fire burned in 2002 approximately 2600 ha in the south east part of the study area.

The Blue Mountain region is characterized by a dry climate, with average annual precipitation from 305 mm to 1270 mm. Elevation ranges

between 500 m and 2700 m. Forest types include spruce (*Picea engelmannii* Parry ex Engelm.) and grand fir (*Abies grandis* [Douglas ex D. Don] Lindl.) at the higher elevations to mixed conifer at mid elevations, to ponderosa pine (*Pinus ponderosa* Douglas ex P. Lawson & C. Lawson) at lower elevations (Franklin et al., 2002). Hardwood species such as black cottonwood (*Populus trichocarpa* Torr. & Gray), quaking aspen (*Populus tremuloides* Michx.), and willow (Salix spp.) occur mainly in the riparian areas and wetlands.

2.2. Lidar-based biomass data

In this study we used AGB estimated from small-footprint, discrete-return lidar data and field measurements for training and testing Landsat-based prediction models. Field data were acquired for fifty-one 15-m radius plots during the summer of 2009 distributed across the lidar area (Fig. 1). Field measurements included diameter at breast height (dbh), species, and height of all live trees with dbh > 2.5 cm. For each tree, total AGB (oven-dry weight) was estimated using ten allometric models developed for regional applications (Jenkins, Chojnacky, Heath, & Birdsey, 2003) and then totaled over the plot area to obtain estimates of biomass density (Mg ha^{-1}). Field-based biomass estimates are subject to several sources of uncertainty including measurement errors and uncertainties in the allometric models. Here, we ignore these uncertainties assuming their magnitude is negligible relative to plot-to-plot variability.

Airborne lidar data were acquired between 19–28 August 2008 with a Leica ALS50 Phase II laser system at an altitude of approximately 900 m. Flight lines overlapped at least 50% on each side. The lidar sensor operated at a wavelength of 1064 nm and recorded pulse range and intensity at a nominal pulse density of >8 pulses per m^2. Up to 4 returns per pulse were recorded. To obtain estimates of vegetation height a 1-m DEM (provided by the vendor) was subtracted from the pulse elevations. Lidar returns co-located with the field plots were then extracted and metrics describing the height and intensity distributions were computed. For a more detailed description of the field and lidar data processing see Pflugmacher et al. (2012).

To map AGB from lidar data we used the regression model from Pflugmacher et al. (2012) built with the same field measurements and lidar data. The model predicts AGB from a canopy volume metric (HVOL), which was calculated as the product of lidar canopy cover (returns above 2 m divided by all returns) and mean lidar vegetation height. The AGB model described 87% of the variation in measured live tree biomass (up to 354 Mg ha^{-1}) with an RMSE = 35.3 Mg ha^{-1}. We applied the model at a raster grid size of 30-m × 30-m comparable to the field plot size. The predicted AGB surface was then smoothed with a mean filter using the same 3 by 3 window to match the Landsat time series processing.

2.3. Landsat data

2.3.1. Image selection and processing

We obtained Landsat MSS, TM, and ETM+ images for the study region (WRS-2 path/row: 43/29) for nearly every year between 1972 and 2010 from the Landsat archive (http://glovis.usgs.gov). To minimize inter-annual changes in sun angle and phenology we selected only images acquired between mid-July and August. Prior to 1984, Landsat MSS data were acquired using a different reference system. For those we obtained overlapping scenes from WRS-1 path/row 46/29 (Fig. 1; Table 4, Pflugmacher et al., 2012).

To quantify biophysical changes associated with forest disturbances and recovery it was crucial that all images in the Landsat time series be geometrically and radiometrically consistent (Lu, Mausel, Brondizio, & Moran, 2004; Song, Woodcock, Seto, Lenney, & Macomber, 2001). Thus, we radiometrically normalized each image to an atmospherically corrected (Chavez, 1996) reference image (here we used 1997) using the MADCAL algorithm of Canty, Nielsen, and Schmidt (2004). Schroeder, Cohen, Song, Canty, and Yang (2006) describe the procedure for MADCAL processing of TM/ETM+ image stacks in more detail.

Including MSS data in the image time series required additional steps (Pflugmacher et al., 2012). Although the majority of the MSS imagery had been orthorectified, additional corrections were necessary to improve the geometric consistency. We utilized an automated program by Kennedy and Cohen (2003) to register all MSS data to the 1997 reference image (RMSE < 0.5 pixel) and resampled each image to 30-m × 30-m. Following Powell, Cohen, Yang, Pierce, and Alberti (2008), we applied the tasseled cap (TC) transformation to the TM/ETM+ data and the MSS data and then normalized MSS to the TM reference image using the TC components brightness (TCB) and greenness (TCG). For TM/ETM+ we used the TC coefficients for reflectance data from Crist (1985). For MSS we used the coefficients from Kauth, Lambeck, Richardson, Thomas, and Pentland (1979) but adjusted for the recent MSS radiometric calibration (Pflugmacher et al., 2012). Residual systematic differences across sensors were corrected by aligning the MSS time series using pixel-level correction factors obtained from overlapping MSS and TM images between 1984 and 1992 (Pflugmacher et al., 2012). We then built annual time series following the LandTrendr method (Kennedy, Yang, & Cohen, 2010). If multiple images were available for a given year, we selected the cloud-free pixels closest to the median Julian day (day 216), and pixels from TM were chosen over pixels from MSS sensors. Finally, we computed TC angle (TCA) from TCG and TCB as described in Powell et al. (2008) as TCA = arctan(TCG/TCB), and TC distance (TCD) first described in Duane et al. (2010), where $TCD = \sqrt{TCG^2 + TCB^2}$. TCA and TCD translate the brightness–greenness plane of the TC transformation into a

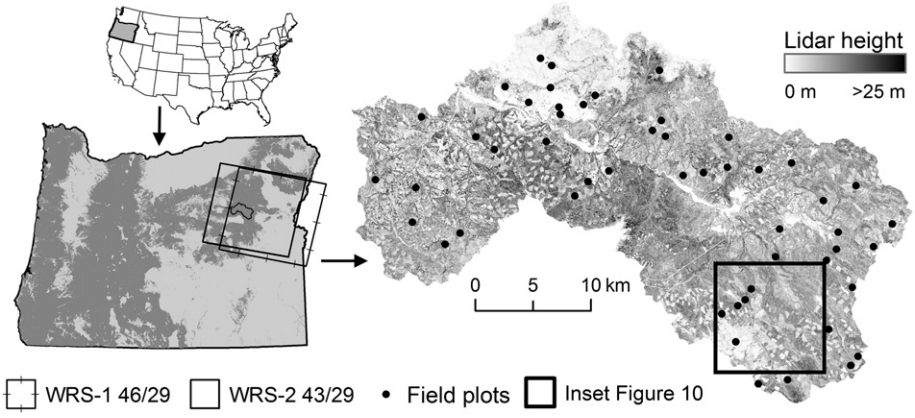

Fig. 1. Map of study area (modified from Pflugmacher et al., 2012).

polar coordinate system. TCA describes a gradient of percent vegetation cover and TCD is related to vegetation composition and structure.

2.3.2. Time-series trajectories

To identify and characterize spectral trends for each pixel, we use the LandTrendr algorithm developed by Kennedy et al. (2010). LandTrendr is a temporal segmentation and fitting algorithm that models change trajectories as a series of sequential line segments. The algorithm seeks to reduce interannual noise caused by variations in phenology and atmospheric conditions, while maintaining the temporal patterns associated with disturbance and recovery. Starting with a predefined maximum number of segments the algorithm iteratively loops through less complex model solutions. The final segmentation is selected from all possible solutions, balancing an increase in residual error with decreasing model complexity (for details see Kennedy et al., 2010). As a result, the trajectory of a pixel may be described by a single segment (i.e., stable, gradual increase or decrease) or by multiple interconnected segments (up to the maximum defined number, here we used six). Likewise, individual change processes may be represented by a single segment or by multiple segments where changes are non-linear (e.g. recovery).

LandTrendr consists of two main steps: temporal segmentation and trajectory fitting. The segmentation step estimates the years (vertices) at which changes begin and end, whereas the trajectory fitting yields estimates of spectral values associated with the detected vertices. In our previous study, we used a single index (TCA) for the segmentation and fitting. Here, we also used TCA to derive the segmentation, but we then fitted TCA and TCD time series to that segmentation. The results were two fitted trajectories, TCA and TCD, with matching temporal patterns (same timing and duration of change processes), but with different spectral responses (e.g. magnitude of changes). For all time-series analyses we used the mean value of a 3 by 3 sliding window to minimize misregistration errors.

2.3.3. Disturbance history metrics

From the fitted trajectories we calculated a series of metrics to characterize the disturbance and recovery (DR) history of each pixel. With TCA and TCD, downward trending trajectory segments represent disturbance and upward trending segments represent recovery. Flat segments represent spectral stability (Fig. 2i). First, we identified the greatest disturbance as the segment with the greatest negative change magnitude (segment b, Fig. 2i). Magnitude was calculated as the difference in spectral value between the start vertex and end vertex of a segment. For the greatest disturbance, the start vertex signifies the pre-disturbance spectral value (vertex B) and the end vertex the post-disturbance spectral value (vertex C). The segments preceding and following the disturbance define the pre-disturbance trend (segment a) and post-disturbance trend (recovery segment c), respectively. Time since the start of the greatest disturbance was calculated by subtracting the year of vertex C from that of vertex E. The approach to calculate DR metrics from LandTrendr trajectories is also described in Kennedy et al. (2012) and Pflugmacher et al. (2012) but here we included several additional metrics.

In this study, we computed 23 DR metrics. From these 23 metrics, 17 were computed twice (for TCA and for TCD trajectories) resulting in a total of 40 potential DR predictor variables (Table 1). Because many metrics describe similar aspects, it was convenient to group them into five main categories: 1) greatest disturbance trend (GD), 2) pre-disturbance trend (BD), 3) post-disturbance trend (i.e. recovery, AD), 4) last monotonic trend (LM), and 5) spectral values (CC) and trend (CT) at the time of prediction. The last monotonic trend summarizes all segments having the same direction prior to the prediction year. Recovery is a positive post-disturbance trend but often recovery is non-linear and spans across multiple segments. Thus, we also estimated total recovery by calculating the spectral change that occurred between the prediction date and the year immediately after disturbance (and

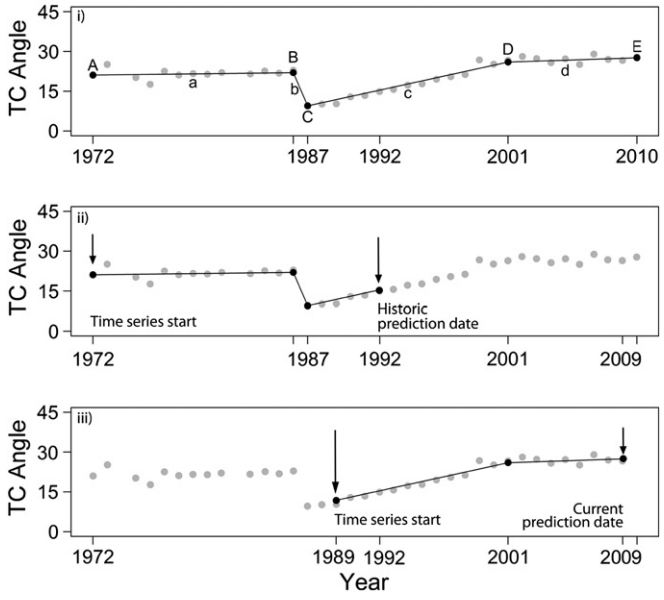

Fig. 2. Example of a Landsat time series for a single pixel over: i) the entire image time series, ii) a period of 20 years from a historic prediction date in 1992, and iii) a period of 20 years from the current prediction date in 2009. Shown are the yearly tasseled cap angle values (grey dots), the fitted segments (black lines), and the segment's vertices (black dots).

five years after disturbance). To describe early recovery dynamics, we calculated the spectral value five years after disturbance, and the change in magnitude in the first five recovery years as in Kennedy et al. (2012). We did not include information on disturbance agent (e.g. fire, harvest, insect) as we did in our previous study (Pflugmacher et al., 2012) because this information was not yet available for the entire study area.

The DR metrics were calculated for all forested pixels including non-disturbed pixels. Doing this enabled us to develop and apply a single model across all trajectory types, i.e. disturbance followed by recovery, disturbance without recovery, recovery only, and no-change. But to apply DR metrics for each trajectory additional rules were required. For pixels characterized by initial recovery and no disturbance, the disturbance start and end year were set to the first year in the time series. As a result, disturbance magnitude and duration were assumed to be zero. If the first segment showed the greatest negative magnitude the disturbance start was set to the first year in the time series. In this case, pre-disturbance magnitude and duration were set to zero and pre-disturbance spectral value was set to the first value in the time series. Similarly, for pixels with negative trends without recovery, the disturbance end was assumed to be the last year in the time series, and post-disturbance magnitude and duration were set to zero. To calculate the 5-year recovery metrics for pixels disturbed within the last five years from the end of the time series, we estimated the recovery magnitude based on the remaining time series length. While this approach avoids the need for stratification by trajectory type, it may lead to higher uncertainties for pixels disturbed during the first or last years in the time series. Because few disturbances occurred in our region within the first year and last eight years, the overall effect on our results was assumed to be minimal.

2.4. Forest inventory data

We used field data from the Continuous Vegetation Survey (CVS) of the Pacific Northwest Region (available from the US Forest Service) to assess predictions of historic AGB and AGB change (Table 2). CVS collect field measurements for all forest land using plots established on systematic grids. Plots are periodically remeasured enabling estimates of

Table 1
Correlation between Landsat-based predictor variables and (log-transformed) lidar-based aboveground biomass (AGB_{Lidar}) (grey shades range from white – no correlation to dark grey – strong correlation). Predictors include disturbance-recovery (DR) metrics and single-date (SD) metrics.

Predictor variable	Description	Abbr.	Correlation with $log(AGB_{Lidar})$	
DR metric			**TCA-fitted**	**TCD-fitted**
Greatest disturbance (GD)	Duration (GDTSE-GDTSS)	GDDUR	0.14	
	Magnitude (BDVAL-ADVAL)	GDMAG	-0.63	0.35
	Relative magnitude (GDMAG/BDVAL)	GDRCH	-0.71	0.37
	Rate of change (GDMAG/GDDUR)	GDROC	-0.66	0.33
	Time since disturbance start	GDTSS	0.41	
	Time since disturbance end	GDTSE	0.25	
Pre-disturbance (BD)	Spectral value	BDVAL	0.23	0.00
	Magnitude	BDMAG	-0.21	-0.02
	Duration	BDDUR	-0.23	
	Rate of change (BDMAG/BDDUR)	BDROC	-0.03	0.13
Post-disturbance (AD)	Spectral value	ADVAL	0.73	-0.27
	Magnitude	ADMAG	-0.31	-0.54
	Duration	ADDUR	0.05	
	Rate of change (ADMAG/ADDUR)	ADROC	0.18	0.42
	Spectral value 5 years after disturbance	ADVA5	0.61	-0.58
	5-year magnitude (ADVA5-ADVAL)	ADMG5	-0.37	-0.60
	Total recovery ((CCTC[A/D]-ADVAL)/ADVAL)	ADREC	-0.09	-0.57
	Total recovery after 5 years ((CCTC[A/D]-ADVA5)/ADVA5)	ADRE5	-0.07	-0.38
Last monotonic trend (LM)	Duration	LMDUR	0.35	
	Magnitude	LMMAG	-0.37	-0.49
	Rate of change (LMMAG/LDDUR)	LMROC	-0.39	-0.40
Current condition (CC)	TC angle	CCTCA	0.29	–
	TC distance	CCTCD	–	-0.77
Current trend (CT)	Rate of change	CTROC	0.35	0.24
SD metric				
Current condition (CC)	TC brightness	CCTCB	-0.76	
	TC greenness	CCTCG	-0.33	
	TC angle	CCTCA	0.29	
	TC distance	CCTCD	-0.77	

biomass change. In our study region, 87 CVS plots were first measured between 1993 and 1996 and then remeasured between 1997 and 2007.

Within each inventory plot, trees ≥ 2.54 cm diameter at breast height (dbh) were measured and the species recorded. We estimated biomass of live trees using the same allometry that we used to estimate AGB from our field data and AGB_{Lidar} (Jenkins et al., 2003). Plot-level biomass densities (Mg ha^{-1}) were then obtained using the recorded trees-per-area expansion factors. We only selected homogenous plots with single conditions (as recorded by the inventory) to minimize misregistration effects. Further, we visually screened plots for outliers associated with edge effects such as adjacent meadows or roads. This removed less than 5% of inventory plots. Finally, for each field plot we extracted the spectral values and time-series metrics associated with the 30-m × 30-m Landsat pixel that contained the plot center. Because a 3 by 3 mean filter had been applied to all spatial data, the effective ground area sampled was 90-m × 90-m around the plot center.

Table 2
Summary statistics of the Current Vegetation Survey (CVS) data.

Assessment period	# Plots	AGB mean (Mg/ha)	AGB SD (Mg/ha)	AGB range (Mg/ha)	Dominant age mean	Dominant age range
1993–1996	87	99.0	55.3	9.0–360.3	95	39–225
1997–2007	87	100.5	51.2	3.3–294.3	91	26–233

2.5. AGB model development

We built empirical models between AGB_{Lidar} (response) and the Landsat-based metrics (predictors) (Table 1) using random forest (RF) (Breiman, 2001). RF does not make distributional assumptions and is

able to account for complex, non-linear interactions among variables. RF improves on traditional tree-based methods by incorporating two random components: 1) each tree is constructed from a bootstrap subsample of the data, and 2) node splits are performed using a random subset of predictor variables. As a result RF does not require tree pruning and independent estimates can be obtained by applying models to the left-out data (referred to as out-of-bag (OOB) data). To develop AGB models, we followed these general steps: i) sampling of model training and testing data, ii) evaluation of the importance of predictor variables, iii) model selection, and iv) model evaluation. We performed all statistical analyses using the R statistical language (R Development Core Team, 2011) and the RandomForest package from (Liaw & Wiener, 2002).

2.5.1. Sampling

To decrease the large data volume and minimize spatial autocorrelation, we sampled the predictor and response (lidar-predicted AGB) raster using a Cartesian grid with a spacing of 500 m. Meadows and other areas that were not forested between 1985 and 2009 were excluded from analyses. To create a forest mask we performed an iso-cluster classification iteratively on a six-band image stack build from TCB, TCG, and TCW for 1985 and 2009, respectively, and visual interpretations of airphotos.

We explored the effect of sampling density on prediction accuracy of Landsat-based AGB by sampling the predictor and response raster using systematic grids ranging from 500 m to 5000 m spacing in 100-m intervals. For each sampling density, we estimated the prediction accuracy using the RMSE of OOB-predicted versus observed AGB_{Lidar}. The RMSE is the generalization error associated with a particular dataset or estimator, and therefore also subject to sampling error. To minimize and capture the uncertainties associated with the sampling, we collected multiple independent samples for each sampling density and calculated the pooled (mean) RMSE and standard error (SE) over all samples. SE was estimated by the standard deviation of the RMSE samples divided by the square root of the sample size. To obtain multiple samples we iteratively offset each grid's starting point by 120, 240, and 360 m in each direction. This produced nine independent samples of size n for each density level. Note that we did not account for uncertainties in the lidar-based prediction; thus the absolute RMSE's are likely underestimated relative to field-based AGB estimates.

2.5.2. Variable importance

We examined the importance of each Landsat predictor variable using the RF importance metric for continuous variables and correlation analysis. RF quantifies importance based on the influence of each variable on the prediction error of each tree. Specifically, RF computes the average increase in MSE (%IncMSE) by permuting the OOB data for a variable while keeping the other predictors constant. The increase in MSE is then averaged over all trees and normalized by the standard deviation. The RF importance metric is therefore a measure of relative importance and influenced by potentially complex interactions between predictors. The metric is often used as a means for variable reduction but interpretation can be challenging, e.g. predictors may rank low when highly correlated with higher-ranking predictors. Additionally, we also explored the relationships between single Landsat predictor variables and AGB_{Lidar} by means of correlation analysis. Here, we log-transformed AGB_{Lidar} to linearize the relationships.

2.5.3. Model selection

To evaluate the performance of disturbance and recovery metrics, we built two prediction models based on: 1) spectral indices from single-date Landsat data (SD, Table 1), and 2) disturbance and recovery metrics in addition to spectral indices (DR, Table 1). Based on the RF importance score we selected only the most influential predictors from the 40 DR metrics for inclusion in the final DR model. This step was not required for prediction, because RF is robust against overfitting (Breiman, 2001), but it can facilitate model interpretation.

To build the single-date model we also used TC indices as predictor variables. We did not include additional indices or spectral bands, as the TC components together commonly explain the majority of the variance in the Landsat spectral space, e.g. 97% in a study from Huang, Wylie, Homer, Yang, and Zylstra (2002). Here, we selected as predictor variables the TCA and TCD values of the current condition, which were also used as DR predictors, but we also included TCB and TCG. We did not include TC wetness (TCW), because this index is not available for Landsat MSS data. Also, in a previous study over the same study area, TCW did not significantly increase the variance explained by a model that predicted field-based AGB from TCB (Pflugmacher et al., 2012). However, the importance of TCW might be different in other regions.

2.5.4. Model evaluation

The models were evaluated based on goodness of fit, prediction accuracy, and by examining model residuals. We calculated the pseudo R^2, which is the mean of the individual bootstrap R^2. To assess a model's performance we computed the RMSE, estimated bias (mean predicted AGB minus mean observed AGB), variance ratio (standard deviation of predicted AGB divided by standard deviation of observed AGB) (Cohen, Maiersperger, Gower, & Turner, 2003), correlation coefficient (r), and slope of the regression line between predicted versus observed AGB. Model performance was evaluated using the same dataset for model training and validation. Independent predictions were obtained by applying each model to the RF OOB data. The method is therefore analogous to cross-validation.

2.6. Prediction of historic biomass and biomass change

We estimated historic AGB and biomass change (ΔAGB) using the single-date model and the disturbance-metric model. The metrics used to build the disturbance model were based on time series from 1972 to 2009 (Section 2.5.3). The year 2009 was selected as the current prediction date to match the lidar acquisition date. To predict historic AGB, we applied each model to historic dates. This meant that the DR metrics had to be recalculated for each pixel to capture only trends prior to each prediction date. For example, if predictions for 1992 were desired then DR metrics were calculated from the 20-year time series between 1972 and 1992 (Figure 2ii). Estimates of ΔAGB were obtained by subtracting predictions between two points in time. We evaluated the historic predictions by comparing the Landsat-predicted biomass changes (ΔAGB_{SD} and ΔAGB_{DR}) with biomass changes from re-measured CVS plots (ΔAGB_{CVS}).

2.7. Influence of time-series length

When predictions for historic time periods are desired, the prediction date moves to an earlier time step and the length of the time series decreases accordingly (Fig. 2ii). Because shorter time series may include less information on disturbance and recovery, it was of interest to explore how decreasing time-series length may influence prediction accuracy of the disturbance-metric model. To explore this, we iteratively decreased the time-series length (L) by 1 year from the original 38 years to 2 years. For each L we fitted a new model using the same DR predictors and assessed its performance based on model R^2 and RMSE. Note, if $L = 1$ then historic information is not included as in the case of the single-date model. Also, because the prediction date, as the last year in the time series, was fixed by the lidar data acquisition year (2009), we decreased the time series length by increasing the time series start year, i.e. from 1972 ($L = 38$) to 2008 ($L = 2$). Fig. 2iii shows an example for $L = 20$ years.

The efficiency of the disturbance model likely depends on the intensity and speed of the ecosystem response to a disturbance and also

the intensity and frequency of past disturbances. In other words, if a disturbance occurred 30 years ago then time series of 30+ years may be needed to describe a highly resilient system or less if spectral recovery is slow or delayed. To explore if varying time series length might have captured different historic disturbance patterns, we analyzed the temporal distribution of abrupt, intense disturbances between 1972 and 2009. We defined *abrupt* as an instantaneous change from one year to another. However, when clouds or missing image years coincide with abrupt events the recorded disturbance duration will increase accordingly. Thus, to account for this 'missing value' artifact we selected all disturbances with a recorded duration of 1 or 2 years. Further, we defined *intense* based on an estimated relative change magnitude greater than 30%. This threshold corresponded to a relative change in lidar-estimated canopy cover of about 50%.

3. Results

3.1. Variable importance

Several Landsat predictor variables showed a correlation with the log-transformed (*ln*) AGB_{Lidar} (Table 1). Based on the current-date spectra, TCD showed a strong correlation with $ln(AGB_{Lidar})$. TCA was only weekly correlated with $ln(AGB_{Lidar})$, although the relationship improved for biomass densities greater than 50 Mg ha^{-1} ($r = 0.59$). However, historic TCA metrics associated with the greatest disturbance spectra and disturbance magnitude (particularly relative change magnitude) were strongly correlated with $ln(AGB_{Lidar})$. The best historic metrics based on TCD characterized post-disturbance trends suggesting that TCD may have captured recovery better than TCA. For example, an increase in AGB_{Lidar} was associated with a decrease in TCD within five years after disturbance. A slightly lower correlation was observed for recovery magnitude measured across the whole length of the post-disturbance segment, and also when a linear trend towards the current date was used. Interestingly, while biomass was correlated with TCA and TCD five years after disturbance, the correlation with TCA was higher immediately after disturbance, whereas the correlation with TCD was higher after five years. Finally, there was only a weak correlation between $ln(AGB_{Lidar})$ and disturbance duration, disturbance time, and pre-disturbance conditions.

The RF importance measures generally agreed with the correlation analysis such that variables that ranked high with respect to variable importance also showed high linear correlations. The most important predictors were current-date TCD (1st) followed by TCA immediately after (2nd) and five years after disturbance (3rd), and relative disturbance magnitude based on TCA (4th). However, some variables with weak linear correlations ranked also high: current-date TCA (5th), TCA before disturbance (8th), relative disturbance magnitude for TCD (9th), and time since disturbance ended (11th).

Overall, the importance of DR metrics declined gradually with the number of variables and did not show a visible break. Therefore, determining a cut-off value to select a parsimonious model was relatively arbitrary. We decided to select the first 10 variables, but also included time since disturbance, since this variable has been effective in other studies (Helmer et al., 2010; Lefsky et al., 2005; Li et al., 2011). After removing co-linear variables ($r > 0.8$) the final model included a total of eight variables (Table 3).

3.2. Model comparison

The model based on single-date Landsat data performed relatively well with an $R^2 = 0.68$ and RMSE = 39.6 Mg ha^{-1}. Including disturbance and recovery metrics improved overall model performance ($R^2 = 0.82$ and RMSE = 30.3 Mg ha^{-1}), but particularly in the high and low biomass range, increasing the dynamic range of the predictions (Fig. 3). Areas of low biomass corresponded mostly with recently disturbed areas, e.g. the two large fires in the north and south of the area and clear-cuts. Here, the single-date model overestimated AGB resulting from regrowth. Both Landsat models slightly underpredicted biomass, although the estimated bias was lower for the disturbance model (Table 3).

3.3. Sampling density

We evaluated the effect of sampling density on prediction accuracy for single-date model and the disturbance-metric model. Varying sampling density between grid spacings of 500 m and 1 km did not affect prediction errors (e.g. $RMSE_{DR,500m} = 30.5 \pm 0.2$ and $RMSE_{DR,1000m} = 31.4 \pm 0.3$). This suggests that a 500-m sampling density was adequate in this study, and that higher densities (<500 m) would not have significantly improved model predictions. On average, the disturbance model performed consistently better than the single-date model across all sampling densities. However, the disturbance model was more sensitive to decreasing sampling density: RMSE increased by 2.6 Mg ha^{-1} per km compared to 1.2 Mg ha^{-1} per km with the single-date model. At a 2 km spacing, the disturbance model performed still substantially better ($RMSE_{DR} = 35.7 \pm 1.2$, $RMSE_{SD} = 42.1 \pm 1.1$), whereas differences diminished at spacings of 4 km and greater ($RMSE_{DR} = 40.9 \pm 2.3$; $RMSE_{SD} = 44.5 \pm 2.1$).

Decreasing the sampling density from 500 m to 5000 m also substantially increased model uncertainties. Standard error (SE) of RMSE increased from 0.17 to 3.17 (0.54 Mg ha^{-1} average increase per km). However, the increase may also be attributed to the small sample sizes at low sampling densities. Sample sizes decreased from 2285 with 500-m spacing to 148, 35, and 22 samples with 2 km, 4 km, and 5 km spacing, respectively. We did not account for spatial autocorrelation when calculating standard errors. As a result, uncertainties in model predictions may have been underestimated. However, the effect would have been consistent across sampling densities and model types.

3.4. Influence of time-series length

The accuracy of the disturbance-based predictions decreased gradually with decreasing time-series length (L) reaching performance levels more similar to those of the single-date model when only ~2–4 years were used (Fig. 4). The difference in RMSE between the DR and SD model for the full time series ($L = 38$) was 9 Mg ha^{-1}, and decreased exponentially but slowly to 3 Mg ha^{-1} until $L = 4$. Based on a fitted power function of the form $RMSE = a \cdot L^b$, the RMSE declined with increasing L at an estimated rate of $b = -0.084 \pm 0.004$ (95% CI) Mg ha^{-1} per year from an estimated initial ($L = 0$) RMSE of $a = 40.9 \pm 0.5$ Mg ha^{-1} ($R^2 = 0.98$). Model R^2 stayed nearly constant for time-series lengths of $L > 13$ ($R^2 = 0.80$–0.82) after which it decreased and showed a visible change at $L = 14$.

Table 3
Model summaries for predicting AGB_{Lidar} based on single-date indices (SD) and disturbance-recovery metrics (DR) (see Table 1 for description of metrics).

Model	Predictors	R^2	RMSE	RMSE%	Variance ratio	Bias	r
SD	CCTCA, CCTCD, CCTCB, CCTCG	0.68	39.64	34.81	0.82	−7.12	0.76
DR	CCTCD, $ADVAL_{TCA}$, $GDRCH_{TCA}$, CCTCA, $ADREC_{TCD}$, $GDRCH_{TCD}$, $BDVAL_{TCA}$, GDTSE	0.82	30.34	26.65	0.86	−5.38	0.87

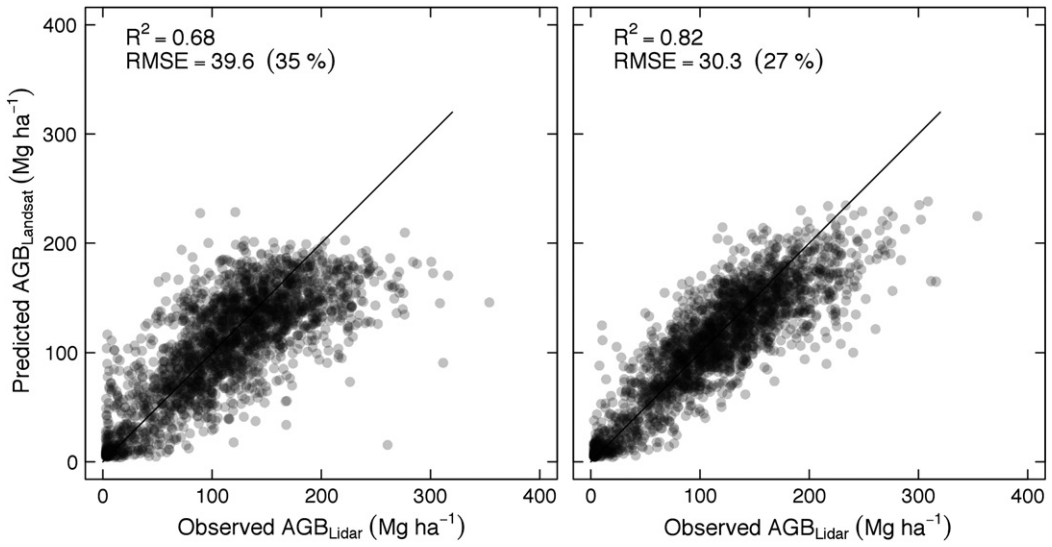

Fig. 3. Predicted (Landsat) versus observed (lidar) aboveground tree biomass (AGB) based on single-date Landsat data (left) and disturbance-recovery metrics (right).

While there was substantial year-to-year variation in the frequency of disturbances between 1972 and 2009 (Fig. 5), two main features were apparent: First, the large wildfire in 1996 coincided with the abrupt decline in R^2 (but not RMSE) at $L = 14$, indicating that knowledge of the fire event and magnitude was important to improve model predictions for the succession following the fire. Second, the frequency of disturbances visibly declined after 2002 ($L = 8$), which also coincided with wildfire in the south of the study area. Thus, for short time series ($L < 8$) changes in AGB were mainly associated with recent forest recovery.

3.5. Historic AGB and AGB change

Estimates of biomass change clearly improved with the inclusion of disturbance metrics ($RMSE_{DR} = 18$ Mg ha^{-1}) compared to the single-date model ($RMSE_{SD} = 24.6$ Mg ha^{-1}) (Fig. 6). Using DR metrics, prediction accuracy improved for low biomass changes (± 25 Mg ha^{-1}) but most importantly for plots that lost more than 50% of their original live biomass. This is a promising result as all disturbed plots had remnant overstory trees and were not completely cleared.

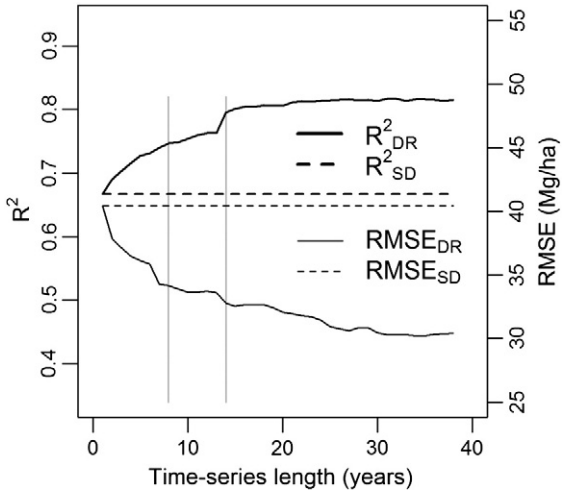

Fig. 4. R^2 (left axis) and RMSE (right axis) as a function of time-series length (L) based on the disturbance-recovery model (DR) and the single-date model (SD). The grey vertical lines mark two significant disturbance events: 1) a large wildfire detected in 1996 ($L = 14$), and 2) a smaller wildfire in 2002 followed by a significant decline in disturbance frequency ($L = 8$).

The application of the disturbance model to historic time periods achieved robust AGB predictions. Prediction errors in the early time periods were comparable to the prediction errors of the more recent time periods. However, the difference between predicted AGB_{DR} and observed AGB_{CVS} was slightly higher in early CVS periods and decreased over time (by 0.84 ± 1.25 Mg ha^{-1} year^{-1}, 95%-CI). This small, residual trend was not statistically significant. Nevertheless, it may indicate that Landsat captured changes in AGB associated with disturbances, but was less effective in describing small gains in AGB associated with tree growth.

4. Discussion

The disturbance and recovery history of forests can be highly complex, particularly when observed over long time periods (Kennedy, Cohen, & Schroeder, 2007). In our study area, forest changes are caused by a range of anthropogenic and natural disturbances of varying intensity and duration (e.g. fire, clear-cuts, partial harvest, insect), and recovery and maturation processes are highly variable. Forest stands may have experienced a single disturbance or multiple disturbances during the observed period. Thus, quantification of the cumulative effects of disturbance history on forest biomass was likely to require a model that captures multiple, consecutive trends (of various direction and duration) that lead to the current condition. In a previous proof-of-concept study (Pflugmacher et al., 2012), we delineated DR trends by means of manual interpretation and hand-digitizing of Landsat time series. Here, we showed that the DR approach can be automated using the trajectory-fitting algorithm LandTrendr (Kennedy et al., 2010) and that it can be used to predict historic AGB and AGB change.

4.1. Using disturbance history for predicting AGB

Landsat-based forest disturbance and recovery metrics were important predictors of AGB. The results are encouraging, especially considering that conifer forests in our study are structurally complex, and disturbances vary substantially with respect to disturbance agent, intensity, and duration (even over a period of 38 years observed here). Including DR metrics improved overall prediction accuracy compared to spectral single-date models by 8% (9.3 Mg ha^{-1}). Whether this estimate will make the difference when it comes to meeting accuracy

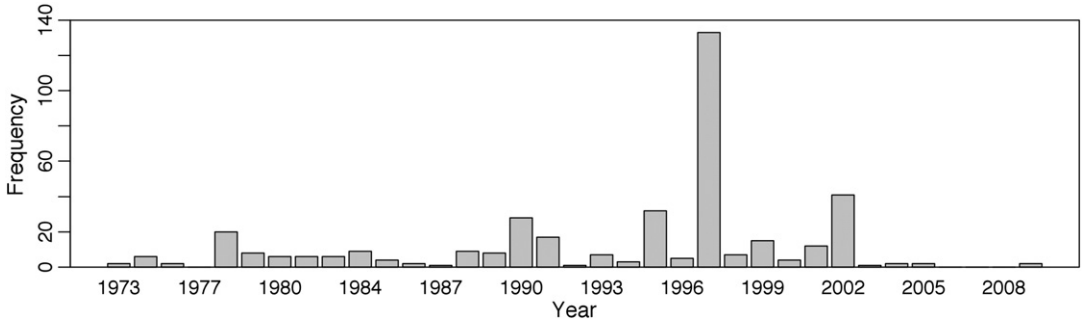

Fig. 5. Number of lidar samples that underwent an abrupt and intense disturbance between 1973 and 2009. The two years with the highest disturbance activity correspond to two wildfires in 1996 (detected in 1997) and 2002, respectively. Also visible are years of increased harvest activity (e.g. 1990 and 1995), and a drastic decrease of disturbances after 2002.

requirements for carbon inventories, it remains to be seen. Most importantly, however, the model improved predictions particularly in low and high biomass stands (up to ~240 Mg ha^{-1}). Overall, the performance of the Landsat spectral data was also relatively good compared to other studies (RMSE% = 34.8%), albeit model predictions saturated at ~200 Mg ha^{-1}.

The dynamic nature of forest disturbances in the region required some simplifications with respect to how disturbance history was characterized. While our approach describes many aspects of temporal trajectories, it favors the greatest disturbance (defined by the magnitude of canopy change). That assumes that the greatest disturbance is the dominant driver for current structure, and that knowledge of the processes or trends immediately before, during, and after are sufficient. This simplification may or may not accuractely characterize stands that are exposed to a multitude of non-stand-replacing change agents over many decades.

Recovery metrics based on TCD trajectories were important descriptors of AGB, but there is no doubt room for improvement. Forest (re-) growth follows more complex and non-linear patterns, which are likely not well captured by our simplified recovery metrics. Non-linear models (e.g. logistic, exponential, and polynomial) are routinely applied to predict height and diameter growth in forest management and planning (Curtis, Herman, & Demars, 1974), but adoption of these concepts to remote sensing data has been slow. A few studies have characterized forest succession using mathematical models (Lawrence & Ripple, 1999; Viedma, Melia, Segarra, & GarciaHaro, 1997; Yang et al., 2005) that can provide ecologically meaningful interpretations of successional development (e.g. mean growth rate and delay in tree establishment). However, these models describe only a small time window associated with (early) forest succession and also do not consider (pre-) disturbance conditions. In comparison, the LandTrendr algorithm characterizes both disturbance and recovery processes simultaneously.

The importance of time since disturbance as a predictor of forest structure seems to vary between disturbance regimes and ecosystems. In this study, time since disturbance was less important for predicting AGB compared to other studies that used Landsat-based disturbance information for predicting forest height, which is correlated with AGB. Helmer et al. (2010) found that forest type and age (estimated from time since disturbance) explained 85% of the variability in forest height in a tropical forest in the Bahamas. However, the authors also showed that using spectral data from the entire time series achieved more realistic results. Li et al. (2011) used the Vegetation Change Tracker (Huang et al., 2010) to estimate stand age and cumulative indices of spectral recovery. The authors then used these metrics to predict forest height estimated with the Geoscience Laser Altimeter System (GLAS) across 11 Landsat scenes covering the US State Mississippi. In their study, stand age explained 90% and the cumulative indices explained 70% of the total variance in GLAS-estimated heights. Hence, time since disturbance appears to be a good predictor of forest structure in systems where stand-replacing disturbances dominate and/or environmental conditions favor rapid growth of relatively few dominant tree species. In our study area, less favorable growing conditions and frequent, low

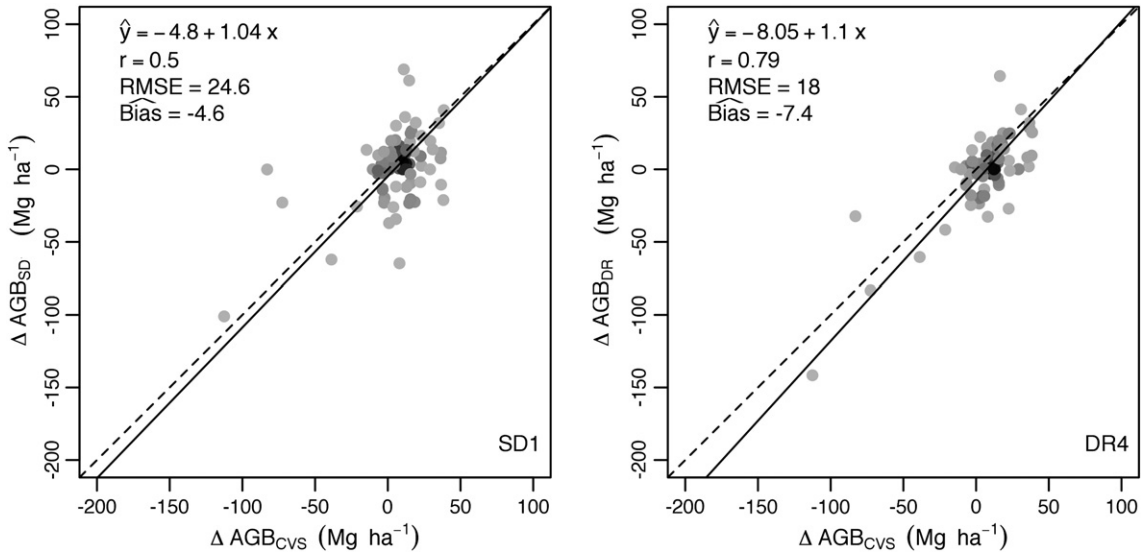

Fig. 6. Change in Landsat-predicted AGB based on single-date Landsat data (left) and disturbance-recovery metrics (right) versus change in AGB from CVS inventories.

intensity disturbances from fires, partial harvest, droughts and insects have created a landscape with a diverse age and stand structure (Campbell, Azuma, & Weyermann, 2003; Johnson, Miyanishi, & Kleb, 1994).

Spatial knowledge of the disturbance agent may improve predictions of AGB. Post-disturbance conditions following wildfires are different from those following clear-cut harvest; the latter are influenced largely by management decisions such as logging intensity and site-preparation practices (Franklin et al., 2002). We did not distinguish between disturbance agents. Mapping disturbance agent has been a difficult task and often involved hand-digitizing (Cohen et al., 2002; Healey et al., 2008). However, research is evolving for automated mapping of disturbance agents across larger landscapes (Kennedy et al., 2012; Schroeder, Wulder, Healey, & Moisen, 2011). Including agent in biomass prediction models is important because agent can be the most valuable predictor of aboveground dead biomass (Pflugmacher et al., 2012), an otherwise illusive biomass component with respect to remote sensing.

To exclude areas that were not forested during the analysis period we used a Landsat-based forest mask. Classification errors in the forest mask may have led to a false inclusion (commission) of some areas with dense shrub vegetation and a false exclusion (omission) of some areas with very sparse tree cover. The potential exclusion of very sparse, low biomass forest pixels and pixels at the forest/non-forest boundary, which are commonly difficult to accurately map, may slightly underestimate the reported errors in the Landsat-based predictions. However, the good agreement between AGB change measured by the forest inventory and predicted by Landsat suggests an overall minor impact on the results of this study.

4.2. Difference between TCA and TCD disturbance history metrics

The correlation analysis between DR predictors and log-transformed (ln) AGB_{Lidar} revealed several important differences between the explanatory value of TCA and TCD trajectories. Log-transformed AGB_{Lidar} was correlated with TCA-based metrics that characterized disturbance intensity and post-disturbance spectral properties, but the same metrics were only weakly correlated with $ln(AGB_{Lidar})$ when based on TCD. Conversely, $ln(AGB_{Lidar})$ was correlated with TCD metrics characterizing recovery processes after disturbance. These results are promising as they indicate that TCD was sensitive to changes in vegetation composition (or quality) associated with different successional pathways, which in turn lead to different biomass accumulation rates. Changes in TCD after disturbance could also indicate changes in understory vegetation caused by low-intensity disturbances. Low intensity fires and thinning eliminate competition for light and nutrients and therefore are likely to promote understory vegetation and tree growth in these systems (Youngblood, Metlen, & Coe, 2006). Conversely, the insensitivity of TCA to the compositional and structural gradient in young forest stands might explain why TCA was only correlated with $ln(AGB_{Lidar})$ at higher biomass densities, and why TCD showed overall higher correlations with $ln(AGB_{Lidar})$.

4.3. Using lidar-predicted AGB for model training

Currently, airborne lidar data provide the most accurate remotely-sensed predictors of forest biomass, but they are not suited for repeated, wall-to-wall monitoring of large areas due to high data acquisition and storage costs. However, as a sampling tool, airborne lidar data can improve the efficiency of field inventories by increasing the number of accurate samples for probability-based biomass estimation (Andersen et al., 2011) or for training prediction models based on other, less accurate but wall-to-wall remote sensing data (Wulder & Seemann, 2003). In this study, airborne lidar data were used to sample a broad range of forest disturbance histories and therefore allowed us to efficiently scale limited (51) field measurements of forest biomass to a larger region.

It is important to note that using predictions of AGB instead of field data directly has consequences. For example, uncertainties in the lidar predictions and also the field data need to be considered to fully describe the uncertainties in the Landsat-based predictions. The lidar model showed a strong fit with the field-estimated AGB data ($R^2 = 0.88$ and RMSE $= 35.3$ Mg ha^{-1}, Pflugmacher et al., 2012). Nevertheless, the presented method reduces the variability in the plot-level AGB values. In some cases this can have a positive effect, but it can also mask the relationship with other variables.

Because lidar-predicted AGB was used for model training and CVS data was used for validating historical predictions, differences between the two data sources could influence the interpretation of the results. Generally, there was good agreement between the two AGB datasets based on 23 CVS plots collected in 2007 over the lidar region ($r = 0.71$). The root-mean-square-difference between AGB_{CVS} and AGB_{Lidar} was 36.9 Mg ha^{-1} (31.6%), which is comparable to the AGB_{Lidar} predictions. However, reduced major axis regression (Cohen et al., 2003) between AGB_{Lidar} and AGB_{CVS} indicated a small, potential systematic difference between the two data sources (slope $= 0.81 \pm 0.19$, 90%-CI; intercept $= 2.30 \pm 26.99$).

4.4. Sampling density

In this study, 500-m to 1000-m grids were adequate to sample the variation in disturbances and biomass within the study area. The optimal sampling density depends on the spatial distribution of disturbances, forest types and structural conditions, and therefore may be different in other areas. However, the results are comparable to those of Hudak et al. (2002), who tested different sampling densities for predicting conifer stand height with (single-date) Landsat data in the dense, more even-aged forests of western Oregon. The authors found that the spatial autocorrelation structure of conifer stands was less than 500 m. Prediction accuracy based on regression models was the highest for 250-m grids, but the 500-m grid achieved comparable results. In fact, in that study, the prediction error did not increase substantially up to 2000-m grid spacing. This suggests that the range of spatial auto-correlation likely did not exceed the smallest interval of our sampling grid.

The accuracy of DR-based models was more sensitive to sampling density than SD-based models. However, DR-based models still performed better than SD-based models using systematic grids of 2-km spacing ($n = 148$). Low sampling densities ($n = 30$) did not capture the variation in disturbance and recovery patterns well enough to substantially improve model predictions compared to SD models. This underlines the importance of sampling design to capture the fine spatial grain of many forest disturbances.

4.5. Influence of time-series length on model predictions

We explored how time-series length affected the strength of the relationship between AGB and DR metrics. The length of time for which effects of DR on current forest structure are meaningful depends on the disturbance frequency and intensity, the rate at which the ecosystem returns to its pre-disturbance state (resilience) and exogenous agents (e.g. climate) that may decouple structural developments from the stand initiating disturbance. Here, we found no clear boundary that would indicate a saturation of the disturbance signal (i.e. ecosystem response). Prediction accuracy gradually increased with increasing time series length across the entire observation period. This suggests that effects of disturbances were still meaningful after 38 years. In fact, vegetation changes and recovery processes occur slowly over long time-scales in our study area. Drought stress in young trees can slow down tree-establishment, and young pine stands can take 10–20 years to reestablish (Law et al., 2001). Prediction accuracy diminished for short time lengths

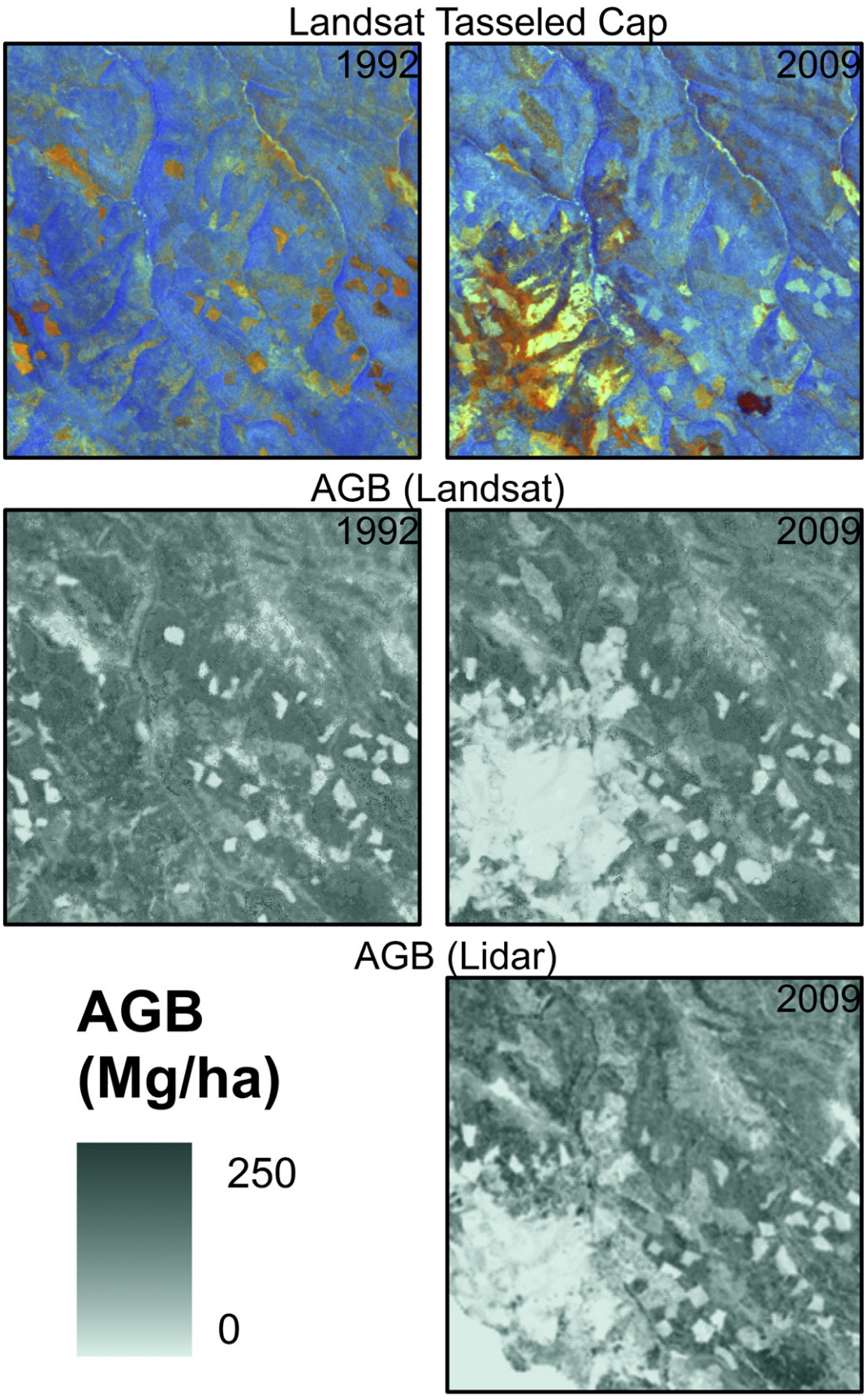

Fig. 7. Zoomed view on the study area (see Fig. 1) showing Landsat tasseled cap (brightness, greenness, wetness) (top row) and AGB predicted from Landsat disturbance-recovery metrics (middle row) for the years 1992 and 2009, and lidar-derived AGB (bottom) for the year 2009. Blue areas in the tasseled cap image represent intact forests, brown and red areas represent stand-replacing disturbances (clear-cut and fire), and brownish colors are associated with partial disturbances (partial harvest and fire).

(<8 years). The substantial decline in management activities and fire in the last decade may have contributed to that. We conclude that, for our study region, observations of at least 10–20 years are necessary to derive strong relationships between Landsat-based DR history and AGB, but even as little as 5 years of history were meaningful. In regions where disturbances are less frequent, longer observations may be needed to capture the disturbance and recovery history.

4.6. Predicting AGB change

By applying DR models back in time, we were able to predict historic AGB and ultimately AGB change in our study area using a combination of field, lidar, and Landsat time-series data. The DR model improved predictions of AGB loss associated with disturbances and it also generally improved predictions of AGB gain associated with tree growth. Thus, the DR model captured AGB dynamics better than the SD model across the whole range of observed change. Further, predictions reflected the spatial and temporal patterns of disturbances and regrowth (Fig. 7).

We demonstrated that the relationships between DR metrics and AGB were generalizable across time periods. The temporal invariance of AGB models based on normalized Landsat time series has previously been demonstrated by Powell et al. (2010) for Landsat models using (single-date) spectral data. The finding that this also applies to disturbance-recovery metrics is encouraging. We observed a small residual (statistically not significant) trend in ΔAGB of 0.84 Mg ha^{-1} year^{-1}, but this estimate is well within the margin of error obtained for AGB predictions (DR: RMSE = 30 Mg ha^{-1}, SD: RMSE = 40 Mg ha^{-1}). Although, we do not know the origin of the estimated bias, it may be related to tree growth in mature or older stands. Because the environmental conditions in our study region are less favorable, tree growth is slow but persistent over long time periods (Law, Sun, Campbell, Van Tuyl, & Thornton, 2003).

Despite the observed limitations, the method presented provides maps of biomass change over large areas that would not have been possible without long-term time series of Landsat data. Ultimately, however, changes in AGB are triggered by a variety of different processes such as changes in land-use, disturbances, regrowth, and changes in metabolic processes driven by environmental conditions. The level of accuracy for which these processes can and need to be observed with remote sensing to improve uncertainties of the global carbon balance is currently vague (Houghton et al., 2009) and likely depends on how these datasets are going to be used in carbon cycle models.

5. Conclusions

Forest biomass mapping with single-date spectral Landsat data has known limitations related to the sensor's diminished sensitivity in closed canopy conditions and the reflectance of bright soils and understory in open forests. Here, we presented a method that directly maps forest AGB and AGB change based on empirical relationships between lidar-estimated AGB and forest disturbance-recovery trajectories from annual Landsat time series between 1972 and 2010. Previously, we showed in a proof-of-concept study that DR metrics (based on TCA trajectories) predicted AGB and other forest structure attributes better than models using single-date Landsat data only. Here, we demonstrated that this approach can be automated across a larger landscape and that it also extends back in time, which is required for estimating biomass change.

Disturbance and recovery metrics were important to estimate AGB. AGB was most correlated with disturbance magnitude metrics from TCA and with post-disturbance recovery from TCD. Previous research has focused on describing disturbance and recovery using a single spectral index (Kennedy et al., 2012; Pflugmacher et al., 2012). Our results highlight that characterization of these processes can be improved when multiple indices are used that describe different spectral gradients associated with vegetation type and structure. TCA and TCD are two complementary indices derived from the same transformation. Used in unison the two indices can improve studies of vegetation change that require long historic observations such as those provided by the Landsat series.

Acknowledgments

This work was supported by NASA Headquarters under the NASA Earth and Space Science Fellowship Program — Grant "NNX10AN49H" and by the Oregon Watershed Enhancement Board. The authors would like to thank Janet Ohmann and Heather Roberts for their valuable help with the CVS data.

References

Aber, J., Neilson, R. P., McNulty, S., Lenihan, J. M., Bachelet, D., & Drapek, R. J. (2001). Forest processes and global environmental change: Predicting the effects of individual and multiple stressors. *Bioscience*, *51*, 735–751.

Abshire, J. B., Sun, X. L., Riris, H., Sirota, J. M., McGarry, J. F., Palm, S., et al. (2005). Geoscience Laser Altimeter System (GLAS) on the ICESat mission: On-orbit measurement performance. *Geophysical Research Letters*, *32*.

Andersen, H. E. (2009). Using Airborne Light Detection and Ranging (LIDAR) to characterize forest stand condition on the Kenai Peninsula of Alaska. *Western Journal of Applied Forestry*, *24*, 95–102.

Andersen, H. E., Strunk, J., Temesgen, H., Atwood, D., & Winterberger, K. (2011). Using multilevel remote sensing and ground data to estimate forest biomass resources in remote regions: A case study in the boreal forests of interior Alaska. *Canadian Journal of Remote Sensing*, *37*, 596–611.

Avitabile, V., Herold, M., Henry, M., & Schmullius, C. (2011). Mapping biomass with remote sensing: a comparison of methods for the case study of Uganda. *Carbon Balance and Management*, *6*, 7.

Baccini, A., Friedl, M.A., Woodcock, C. E., & Warbington, R. (2004). Forest biomass estimation over regional scales using multisource data. *Geophysical Research Letters*, *31*.

Baccini, A., Goetz, S. J., Walker, W. S., Laporte, N. T., Sun, M., Sulla-Menashe, D., et al. (2012). Estimated carbon dioxide emissions from tropical deforestation improved by carbon-density maps. *Nature Climate Change*, *2*, 182–185.

Baldocchi, D.D. (2003). Assessing the eddy covariance technique for evaluating carbon dioxide exchange rates of ecosystems: past, present and future. *Global Change Biology*, *9*, 479–492.

Blackard, J. A., Finco, M. V., Helmer, E. H., Holden, G. R., Hoppus, M. L., Jacobs, D.M., et al. (2008). Mapping US forest biomass using nationwide forest inventory data and moderate resolution information. *Remote Sensing of Environment*, *112*, 1658–1677.

Blair, J. B., Rabine, D. L., & Hofton, M.A. (1999). The Laser Vegetation Imaging Sensor: a medium-altitude, digitisation-only, airborne laser altimeter for mapping vegetation and topography. *ISPRS Journal of Photogrammetry and Remote Sensing*, *54*, 115–122.

Bonan, G. B. (2008). Forests and climate change: Forcings, feedbacks, and the climate benefits of forests. *Science*, *320*, 1444–1449.

Boudreau, J., Nelson, R. F., Margolis, H. A., Beaudoin, A., Guindon, L., & Kimes, D. S. (2008). Regional aboveground forest biomass using airborne and spaceborne LiDAR in Québec. *Remote Sensing of Environment*, *112*, 3876–3890.

Breiman, L. (2001). Random forests. *Machine Learning*, *45*, 5–32.

Campbell, S., Azuma, D., & Weyermann, D. (2003). Forests of Eastern Oregon: An overview. U.S. Department of Agriculture, Forest Service, Pacific Northwest Research Station.

Campbell, S., & Liegel, L. (1996). Disturbance and forest health in Oregon and Washington. Portland: OR: U.S. Department of Agriculture Forest Service Pacific Northwest Research Station, Pacific Northwest Region, Oregon Department of Forestry, Washington Department of Natural Resources.

Canty, M. J., Nielsen, A. A., & Schmidt, M. (2004). Automatic radiometric normalization of multitemporal satellite imagery. *Remote Sensing of Environment*, *91*, 441–451.

Chavez, P. S. (1996). Image-Based Atmospheric Corrections - Revisited and Improved. *Photogrammetric Engineering and Remote Sensing*, *62*, 1025–1036.

Cohen, W. B., & Goward, S. N. (2004). Landsat's role in ecological applications of remote sensing. *Bioscience*, *54*, 535–545.

Cohen, W. B., Harmon, M. E., Wallin, D. O., & Fiorella, M. (1996). Two decades of carbon flux from forests of the Pacific Northwest — Estimates from a new modeling strategy. *Bioscience*, *46*, 836–844.

Cohen, W. B., Maiersperger, T. K., Gower, S. T., & Turner, D. P. (2003). An improved strategy for regression of biophysical variables and Landsat ETM + data. *Remote Sensing of Environment*, *84*, 561–571.

Cohen, W. B., Spies, T. A., Alig, R. J., Oetter, D. R., Maiersperger, T. K., & Fiorella, M. (2002). Characterizing 23 years (1972–95) of stand replacement disturbance in western Oregon forests with Landsat imagery. *Ecosystems*, *5*, 122–137.

Coops, N. C., & Waring, R. H. (2001). The use of multiscale remote sensing imagery to derive regional estimates of forest growth capacity using 3-PGS. *Remote Sensing of Environment*, *75*, 324–334.

Crist, E. P. (1985). A TM tasseled cap equivalent transformation for reflectance factor data. *Remote Sensing of Environment*, *17*, 301–306.

Curtis, R. O., Herman, F. R., & Demars, D. J. (1974). Height growth and site index for Douglas-Fir in high-elevation forests of Oregon Washington cascades. *Forest Science*, *20*, 307–316.

Denman, K. L., Brasseur, G., Chidthaisong, A., Ciais, P., Cox, P.M., Dickinson, R. E., et al. (2007). Couplings between changes in the climate system and biogeochemistry. In

S. Solomon, D. Qin, M. Manning, Z. Chen, M. Marquis, K. B. Averyt, M. Tignor, & H. L. Miller (Eds.), *Climate change 2007: The physical science basis. Contribution of working group i to the fourth assessment report of the intergovernmental panel on climate change*. Cambridge, United Kingdom and New York, NY, USA: Cambridge University Press.

Development Core Team, R. (2011). R: A language and environment for statistical computing. Vienna, Austria: R Foundation for Statistical Computing.

Drake, J. B., Dubayah, R. O., Clark, D. B., Knox, R. G., Blair, J. B., Hofton, M.A., et al. (2002). Estimation of tropical forest structural characteristics using large-footprint lidar. *Remote Sensing of Environment*, *79*, 305–319.

Duane, M. V., Cohen, W. B., Campbell, J. L., Hudiburg, T., Turner, D. P., & Weyermann, D. L. (2010). Implications of alternative field-sampling designs on Landsat-based mapping of stand age and carbon stocks in Oregon forests. *Forest Science*, *56*, 405–416.

Dubayah, R. O., Sheldon, S. L., Clark, D. B., Hofton, M.A., Blair, J. B., Hurtt, G. C., et al. (2010). Estimation of tropical forest height and biomass dynamics using lidar remote sensing at La Selva, Costa Rica. *Journal of Geophysical Research-Biogeosciences*, *115*.

Franklin, J. F., Spies, T. A., Van Pelt, R., Carey, A.B., Thornburgh, D. A., Berg, D. R., et al. (2002). Disturbances and structural development of natural forest ecosystems with silvicultural implications, using Douglas-fir forests as an example. *Forest Ecology and Management*, *155*, 399–423.

Goetz, S. J., Baccini, A., Laporte, N. T., Johns, T., Walker, W., Kellndorfer, J., et al. (2009). Mapping and monitoring carbon stocks with satellite observations: A comparison of methods. *Carbon Balance and Management*, *4*, 2.

Goodale, C. L., Apps, M. J., Birdsey, R. A., Field, C. B., Heath, L. S., Houghton, R. A., et al. (2002). Forest carbon sinks in the Northern Hemisphere. *Ecological Applications*, *12*, 891–899.

Gough, C. M., Vogel, C. S., Harrold, K. H., George, K., & Curtis, P.S. (2007). The legacy of harvest and fire on ecosystem carbon storage in a north temperate forest. *Global Change Biology*, *13*, 1935–1949.

Gregoire, T. G., Stahl, G., Naesset, E., Gobakken, T., Nelson, R., & Holm, S. (2011). Model-assisted estimation of biomass in a LiDAR sample survey in Hedmark County, Norway. *Canadian Journal of Forest ResearchRevue Canadienne De Recherche Forestiere*, *41*, 83–95.

Hall, R. J., Skakun, R. S., Arsenault, E. J., & Case, B.S. (2006). Modeling forest stand structure attributes using Landsat ETM+ data: Application to mapping of aboveground biomass and stand volume. *Forest Ecology and Management*, *225*, 378–390.

Halpern, C. B. (1988). Early successional pathways and the resistance and resilience of forest communities. *Ecology*, *69*, 1703–1715.

Harmon, M. E., Ferrell, W. K., & Franklin, J. F. (1990a). Effects on carbon storage of conversion of old-growth forests to young forests. *Science*, *247*, 699–702.

Harmon, M. E., Ferrell, W. K., & Franklin, J. F. (1990b). Effects on carbon storage of conversion of old-growth forests to young forests. *Science*, *247*, 699–702.

Healey, S. P., Cohen, W. B., Spies, T. A., Moeur, M., Pflugmacher, D., Whitley, M. G., et al. (2008). The relative impact of harvest and fire upon landscape-level dynamics of older forests: Lessons from the Northwest Forest Plan. *Ecosystems*, *11*, 1106–1119.

Helmer, E. H., Lefsky, M.A., & Roberts, D. A. (2009). Biomass accumulation rates of Amazonian secondary forest and biomass of old-growth forests from Landsat time series and the Geoscience Laser Altimeter System. *Journal of Applied Remote Sensing*, *3*.

Helmer, E. H., Ruzycki, T. S., Wunderle, J. M., Vogesser, S., Ruefenacht, B., Kwit, C., et al. (2010). Mapping tropical dry forest height, foliage height profiles and disturbance type and age with a time series of cloud-cleared Landsat and ALI image mosaics to characterize avian habitat. *Remote Sensing of Environment*, *114*, 2457–2473.

Houghton, R. A. (2005). Aboveground forest biomass and the global carbon balance. *Global Change Biology*, *11*, 945–958.

Houghton, R. A., Hall, F., & Goetz, S. J. (2009). Importance of biomass in the global carbon cycle. *Journal of Geophysical Research-Biogeosciences*, *114*.

Huang, C. Q., Goward, S. N., Masek, J. G., Thomas, N., Zhu, Z. L., & Vogelmann, J. E. (2010). An automated approach for reconstructing recent forest disturbance history using dense Landsat time series stacks. *Remote Sensing of Environment*, *114*, 183–198.

Huang, C., Wylie, B., Homer, C., Yang, L., & Zylstra, G. (2002). Derivation of a tasselled cap transformation based on Landsat 7 at-satellite reflectance. *International Journal of Remote Sensing*, *23*, 1741–1748.

Hudak, A. T., Lefsky, M.A., Cohen, W. B., & Berterretche, M. (2002). Integration of lidar and Landsat ETM plus data for estimating and mapping forest canopy height. *Remote Sensing of Environment*, *82*, 397–416.

Jenkins, J. C., Chojnacky, D. C., Heath, L. S., & Birdsey, R. A. (2003). National-scale biomass estimators for United States tree species. *Forest Science*, *49*, 12–35.

Johnson, E. A., Miyanishi, K., & Kleb, H. (1994). The hazards of interpretation of static age structures as shown by stand reconstructions in a Pinus-Contorta Picea-Engelmannii Forest. *Journal of Ecology*, *82*, 923–931.

Kasischke, E. S., Hyer, E. J., Novelli, P. C., Bruhwiler, L. P., French, N. H. F., Sukhinin, A. I., et al. (2005). Influences of boreal fire emissions on Northern Hemisphere atmospheric carbon and carbon monoxide. *Global Biogeochemical Cycles*, *19*.

Kauth, R. J., Lambeck, P. F., Richardson, W., Thomas, G. S., & Pentland, A. P. (1979). Feature extraction applied to agricultural crops as seen by Landsat. *Technical Session LACIE Symposium* (pp. 705–721). Houston: National Aeronautics and Space Administration.

Kennedy, R. E., & Cohen, W. B. (2003). Automated designation of tie-points for image-to-image coregistration. *International Journal of Remote Sensing*, *24*, 3467–3490.

Kennedy, R. E., Cohen, W. B., & Schroeder, T. A. (2007). Trajectory-based change detection for automated characterization of forest disturbance dynamics. *Remote Sensing of Environment*, *110*, 370–386.

Kennedy, R. E., Yang, Z., & Cohen, W. B. (2010). Detecting trends in forest disturbance and recovery using yearly Landsat time series: 1. LandTrendr — Temporal segmentation algorithms. *Remote Sensing of Environment*, *114*, 2897–2910.

Kennedy, R. E., Yang, Z., Cohen, W. B., Pfaff, E., Braaten, J., & Nelson, P. (2012). Spatial and temporal patterns of forest disturbance and growth within the area of the Northwest Forest Plan. *Remote Sensing of Environment*, *122*, 117–133.

Law, B. E., Kelliher, F. M., Baldocchi, D.D., Anthoni, P.M., Irvine, J., Moore, D., et al. (2001). Spatial and temporal variation in respiration in a young ponderosa pine forests during a summer drought. *Agricultural and Forest Meteorology*, *110*, 27–43.

Law, B. E., Sun, O. J., Campbell, J., Van Tuyl, S., & Thornton, P. E. (2003). Changes in carbon storage and fluxes in a chronosequence of ponderosa pine. *Global Change Biology*, *9*, 510–524.

Lawrence, R. L., & Ripple, W. J. (1999). Calculating change curves for multitemporal satellite imagery: Mount St. Helens 1980–1995. *Remote Sensing of Environment*, *67*, 309–319.

Lefsky, M.A., Cohen, W. B., Acker, S. A., Parker, G. G., Spies, T. A., & Harding, D. (1999). Lidar remote sensing of the canopy structure and biophysical properties of Douglas-fir western hemlock forests. *Remote Sensing of Environment*, *70*, 339–361.

Lefsky, M.A., Cohen, W. B., Harding, D. J., Parker, G. G., Acker, S. A., & Gower, S. T. (2002). Lidar remote sensing of above-ground biomass in three biomes. *Global Ecology and Biogeography*, *11*, 393–399.

Lefsky, M.A., Cohen, W. B., Parker, G. G., & Harding, D. J. (2002). Lidar remote sensing for ecosystem studies. *Bioscience*, *52*, 19–30.

Lefsky, M.A., Cohen, W. B., & Spies, T. A. (2001). An evaluation of alternate remote sensing products for forest inventory, monitoring, and mapping of Douglas-fir forests in western Oregon. *Canadian Journal of Forest ResearchRevue Canadienne De Recherche Forestiere*, *31*, 78–87.

Lefsky, M.A., Turner, D. P., Guzy, M., & Cohen, W. B. (2005). Combining lidar estimates of aboveground biomass and Landsat estimates of stand age for spatially extensive validation of modeled forest productivity. *Remote Sensing of Environment*, *95*, 549–558.

Li, A., Huang, C., Sun, G., Shi, H., Toney, C., Zhu, Z., et al. (2011). Modeling the height of young forests regenerating from recent disturbances in Mississippi using Landsat and ICESat data. *Remote Sensing of Environment*, *115*, 1837–1849.

Liaw, A., & Wiener, M. (2002). Classification and regression by randomForest. *R News*, *2*, 18–22.

Lu, D. S. (2006). The potential and challenge of remote sensing-based biomass estimation. *International Journal of Remote Sensing*, *27*, 1297–1328.

Lu, D., Mausel, P., Brondizio, E., & Moran, E. (2004). Change detection techniques. *International Journal of Remote Sensing*, *25*, 2365–2407.

Masek, J. G., & Collatz, G. J. (2006). Estimating forest carbon fluxes in a disturbed southeastern landscape: Integration of remote sensing, forest inventory, and biogeochemical modeling. *Journal of Geophysical Research-Biogeosciences*, *111*.

Meigs, G. W., Donato, D. C., Campbell, J. L., Martin, J. G., & Law, B. E. (2009). Forest fire impacts on carbon uptake, storage, and emission: The role of burn severity in the Eastern Cascades, Oregon. *Ecosystems*, *12*, 1246–1267.

Meigs, G. W., Kennedy, R. E., & Cohen, W. B. (2011). A Landsat time series approach to characterize bark beetle and defoliator impacts on tree mortality and surface fuels in conifer forests. *Remote Sensing of Environment*, *115*, 3707–3718.

Nelson, R., Krabill, W., & Tonelli, J. (1988). Estimating forest biomass and volume using airborne laser data. *Remote Sensing of Environment*, *24*, 247–267.

Pflugmacher, D., Cohen, W. B., & Kennedy, R. E. (2012). Using Landsat-derived disturbance history (1972–2010) to predict current forest structure. *Remote Sensing of Environment*, *122*, 146–165.

Powell, S. L., Cohen, W. B., Healey, S. P., Kennedy, R. E., Moisen, G. G., Pierce, K. B., et al. (2010). Quantification of live aboveground forest biomass dynamics with Landsat time-series and field inventory data: A comparison of empirical modeling approaches. *Remote Sensing of Environment*, *114*, 1053–1068.

Powell, S. L., Cohen, W. B., Yang, Z., Pierce, J.D., & Alberti, M. (2008). Quantification of impervious surface in the Snohomish Water Resources Inventory Area of Western Washington from 1972–2006. *Remote Sensing of Environment*, *112*, 1895–1908.

Running, S. W., Nemani, R. R., Ann Heinsch, F., Zhao, M., Reeves, M., & Hashimoto, H. (2004). A continuous satellite-derived measure of global terrestrial primary production. *Bioscience*, *54*, 547–560.

Saatchi, S. S., Harris, N. L., Brown, S., Lefsky, M., Mitchard, E. T., Salas, W., et al. (2011). Benchmark map of forest carbon stocks in tropical regions across three continents. *Proceedings of the National Academy of Sciences of the United States of America*, *108*, 9899–9904.

Schroeder, T. A., Cohen, W. B., Song, C., Canty, M. J., & Yang, Z. (2006). Radiometric correction of multi-temporal Landsat data for characterization of early successional forest patterns in western Oregon. *Remote Sensing of Environment*, *103*, 16–26.

Schroeder, T. A., Wulder, M.A., Healey, S. P., & Moisen, G. G. (2011). Mapping wildfire and clearcut harvest disturbances in boreal forests with Landsat time series data. *Remote Sensing of Environment*, *115*, 1421–1433.

Smith, B., Knorr, W., Widlowski, J. L., Pinty, B., & Gobron, N. (2008). Combining remote sensing data with process modelling to monitor boreal conifer forest carbon balances. *Forest Ecology and Management*, *255*, 3985–3994.

Song, C., Woodcock, C. E., Seto, K. C., Lenney, M. P., & Macomber, S. A. (2001). Classification and change detection using Landsat TM data: When and how to correct atmospheric effects? *Remote Sensing of Environment*, *75*, 230–244.

Spies, T. A. (1998). Forest structure: A key to the ecosystem. *Northwest Science*, *72*, 34–39.

Stephens, P. R., Kimberley, M.O., Beets, P. N., Paul, T. S. H., Searles, N., Bell, A., et al. (2012). Airborne scanning LiDAR in a double sampling forest carbon inventory. *Remote Sensing of Environment*, *117*, 348–357.

Urbanski, S., Barford, C., Wofsy, S., Kucharik, C., Pyle, E., Budney, J., et al. (2007). Factors controlling CO2 exchange on timescales from hourly to decadal at Harvard Forest. *Journal of Geophysical Research-Biogeosciences*, *112*.

Viedma, O., Melia, J., Segarra, D., & GarciaHaro, J. (1997). Modeling rates of ecosystem recovery after fires by using Landsat TM data. *Remote Sensing of Environment*, *61*, 383–398.

Wulder, M.A., & Seemann, D. (2003). Forest inventory height update through the integration of lidar data with segmented Landsat imagery. *Canadian Journal of Remote Sensing, 29*, 536–543.

Yang, Z. Q., Cohen, W. B., & Harmon, M. E. (2005). Modeling early forest succession following clear-cutting in western Oregon. *Canadian Journal of Forest ResearchRevue Canadienne De Recherche Forestiere, 35*, 1889–1900.

Youngblood, A., Metlen, K. L., & Coe, K. (2006). Changes in stand structure and composition after restoration treatments in low elevation dry forests of northeastern Oregon. *Forest Ecology and Management, 234*, 143–163.

Zolkos, S. G., Goetz, S. J., & Dubayah, R. (2013). A meta-analysis of terrestrial aboveground biomass estimation using lidar remote sensing. *Remote Sensing of Environment, 128*, 289–298.